Journal of Zhejiang University-SCIENCE A (Applied Physics & Engineering) 2022 23(11):900-916
www.jzus.zju.edu.cn; www.springer.com/journal/11582
E-mail: jzus_a@zju.edu.cn

Research Article

https://doi.org/10.1631/jzus.A2200192

Check for updates

Shaking table tests on a cantilever retaining wall with reinforced and unreinforced backfill

Ming WEI[1], Qiang LUO[1,2], Gui-shuai FENG[1], Teng-fei WANG[1,2]✉, Liang-wei JIANG[1,2]

[1]*School of Civil Engineering, Southwest Jiaotong University, Chengdu 610031, China*
[2]*MOE Key Laboratory of High-Speed Railway Engineering, Chengdu 610031, China*

Abstract: Physical modelling of cantilever retaining walls with and without backfill reinforcement was conducted on a 1*g* shaking table to evaluate the mitigation effect of reinforcement on system dynamics (*g* denotes the acceleration of gravity). The model wall has a height of 1.5 m with a scale ratio of 1/4 and retains dry sand throughout. The input motions are amplified to three levels of input peak base acceleration, 0.11*g*, 0.24*g*, and 0.39*g*, corresponding to minor, moderate, and major earthquakes, respectively. Investigation of the seismic response of the retaining walls focuses on acceleration and lateral displacement of the wall and backfill, dynamic earth pressures, and tensile load in the reinforcements (modeled by phosphor-bronze strips welded into a mesh). The inclusion of reinforcement has been observed to improve the integrity of the wall-soil system, mitigate vibration-related damage, and reduce the fundamental frequency of a reinforced system. Propagation of acceleration from the base to the upper portion is accompanied by time delay and nonlinear amplification. A reinforced system with a lower acceleration amplification factor than the unreinforced one indicates that reinforcement can reduce the amplification effect of input motion. Under minor and moderate earthquake loadings, reinforcement allows the inertia force and seismic earth pressure to be asynchronous and decreases the seismic earth pressure when inertia forces peak. During major earthquake loading, the wall is displaced horizontally less than the backfill, with soil pushing the wall substantially; the effect of backfill reinforcement has not been fully mobilized. The dynamic earth pressure is large at the top and diminishes toward the bottom.

Key words: Cantilever retaining wall; Backfill reinforcement; Seismic response; Shaking table test; Dynamic earth pressure; Phase shift

1 Introduction

During an earthquake, failure of retaining structures can cause significant damage to critical infrastructure. With their simple form, ease of construction, and ability to adapt to lower bearing capacities of foundations, cantilever retaining walls are widely used to retain structures. During the 1995 Hyogoken-Nanbu earthquake, many cantilever retaining walls sustained moderate damage, with seismic performance intermediate between conventional masonry or unreinforced concrete gravity retaining walls and geosynthetic-reinforced soil retaining walls (Tatsuoka et al., 1996). Since then, researchers have investigated the seismic performance of various retaining walls.

There are three primary approaches to seismic studies of retaining walls: the analytical method (Mononobe and Matsuo, 1929; Seed and Whitman, 1970; Veletsos and Younan, 1997; Kamiloğlu and Şadoğlu, 2019), physical modelling (Al Atik and Sitar, 2010; Conti et al., 2012; Ertugrul et al., 2017; Gao et al., 2017; Jo et al., 2017), and numerical simulation (Green et al., 2008; Osouli and Zamiran, 2017). The analytical method relies on ideal assumptions that are not always consistent with reality. Among them, the classical analytical methods include the pseudo-static Mononobe-Okabe (MO) method and the Seed-Whitman (SW) method (Mononobe and Matsuo, 1929; Seed and Whitman, 1970). In numerical simulations, the determination of appropriate boundary conditions and constitutive models is complicated. By contrast, physical modelling is reliable as it can visually and

✉ Teng-fei WANG, w@swjtu.edu.cn
Qiang LUO, https://orcid.org/0000-0003-3229-5125
Teng-fei WANG, https://orcid.org/0000-0003-4079-0687

Received Apr. 2, 2022; Revision accepted July 29, 2022;
Crosschecked Oct. 26, 2022

© Zhejiang University Press 2022

realistically evaluate the dynamic behaviour of retaining walls under earthquake loads (Wood et al., 2002; Eftekhari and Panah, 2021; Kilic et al., 2021; Li et al., 2021; Samee et al., 2022). Nevertheless, physical modeling may exhibit limitations such as failing to strictly satisfy the similarity law, potentially leading to a deviation from reality. To better estimate the performance of prototype structures, a modified similarity law has been proposed (Wood et al., 2002). To date, the seismic physical model testing of the retaining wall primarily involves 1*g* shaking tables and dynamic geotechnical centrifuges (*g* denotes the acceleration of gravity).

Initially, cantilever retaining walls were tested on shaking tables compared to the conventional pseudo-static approaches (Koseki et al., 1998b; Watanabe et al., 2003), but usually on small-scale models. Dynamic centrifuge modelling of a cantilevered retaining wall (Al Atik and Sitar, 2010) showed that due to a phase difference between dynamic earth pressure and wall inertia, the design method with forces simultaneously acting on the retaining wall was excessively conservative. The dynamic earth pressure has a triangular distribution along with the wall height and is smaller than the MO method. Other studies (Wilson and Elgamal, 2015; Jo et al., 2017) also observed that dynamic earth pressures and wall inertia forces are asynchronous. Sand and expanded polystyrene (EPS) composite soil were used as two types of backfill in shake table testing of cantilever retaining walls to compare their effect on dynamic behaviour (Gao et al., 2017). With minor input motions, the magnitude of dynamic earth pressure coincides with the MO method; however, increasing acceleration leads to a larger calculated value than the MO method (Green et al., 2008). The effect of backfill reinforcement on the dynamic response of cantilever retaining walls has received relatively little attention.

Reinforced soil structures perform well under major seismic loading and are widely used in earthworks, such as retaining walls (Krishna and Latha, 2009; Ren et al., 2020; Xu et al., 2021), embankments (Tatsuoka et al., 2007; Edinçliler and Toksoy, 2017; Watanabe et al., 2020), slopes (Ding et al., 2020), and abutments (Zheng et al., 2018; Xu C et al., 2020). Reinforced soil retaining walls are probably the most widely used application of backfill reinforcement technology. Shake table testing of rigid-faced reinforced soil retaining walls with geogrid reinforcement shows that the displacement of the wall facing can be dramatically reduced (Krishna and Latha, 2009). The seismic performance of vertical-faced wrap-around reinforced soil retaining walls with heat-bonded nonwoven geotextile was tested on a 1*g* shaking table (Huang, 2019). The results suggested that the maximum tensile forces due to shaking follow a trapezoidal pattern. The possible reinforcement impact on the seismic response of reinforced soil retaining walls has also been confirmed by other studies (El-Emam and Bathurst, 2007; Wang et al., 2015; Safaee et al., 2021). The inclusion of woven geotextile reinforcements in the embankment model attenuates transmitted acceleration travelling through reinforced embankment models and improves seismic performance (Edinçliler and Toksoy, 2017). Although backfill reinforcement can effectively reduce the seismic response of earth structures, it remains unclear what the seismic behaviour of cantilever retaining walls backfilled with reinforced soil will be.

This study reports two independent groups of 1*g* shaking table tests conducted on a cantilever retaining wall retaining either reinforced or unreinforced soils. A stepped-amplitude harmonic base acceleration record was used as input. The effectiveness of backfill reinforcement behind the cantilever retaining wall was examined against fundamental frequency, time histories of acceleration, acceleration amplification, horizontal displacement of the wall facing and backfill, dynamic earth pressure, and reinforcement load.

2 Experimental procedure

2.1 Shaking table facility and soil container

Physical model testing was carried out at Southwest Jiaotong University, China using a servo hydraulically controlled seismic simulation shaking table. The table vibrates unidirectionally with a frequency range of 0.4 to 15.0 Hz and a maximum displacement of 100 mm. Its maximum thrust and payload are 400 and 250 kN, respectively. The shaking table's loading platform measures 4 m×2 m, and in full load conditions, its peak acceleration amplitude is 1.2*g*.

Modelling was carried out in a rigid steel soil container bolted to the shaking table's loading platform. The rigid soil container has internal dimensions

of 2.1 m high, 3.5 m long, and 1.5 m wide. Steel sections with hollow rectangular sections are welded into the skeleton of the rigid box. For observation of the test phenomenon, the closed end of the container was made from a steel plate in the shaking direction, while the remaining two sides were made from transparent acrylic glass. Furthermore, a 40-mm-thick sheet of expanded polystyrene foam was used inside the closed end of the model box to reduce the reflection of waves on the boundaries. Fig. 1 provides a general view of the shaking table system with its critical mechanical components.

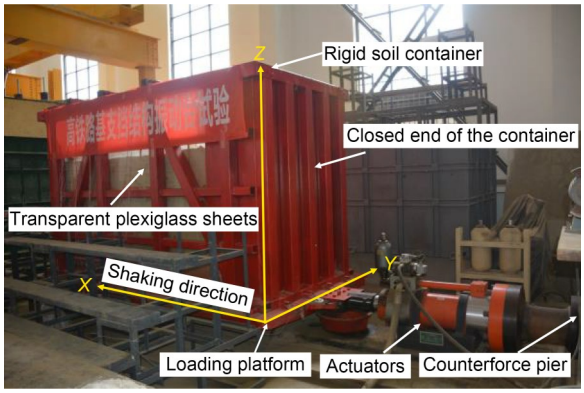

Fig. 1 Rigid soil container mounted on the shaking table

2.2 Scaling laws

As is well known, a reduced-scale physical model needs to adhere to specific similitude laws to replicate the behaviour of its prototype. The scaling laws proposed by Iai (1989) with development (Wood, 2004) were applied in this study. A close relationship exists between soil shear modulus and effective stress. In the 1*g* shaking table test, the effective stress of backfill, however, is lower than the prototype structure. Given the same soil material and unity density employed for the model and prototype, the shear modulus will be different. According to Hardin and Drnevich (1972), a positive relationship exists between the soil shear modulus G and the power function of the effective stress σ' ($G \propto (\sigma')^{\lambda}$). For the soil type, the exponent λ is a dimensionless governing parameter, prescribed, based on practical experience, as 0.5 for sand (Kokusho, 1980; Yu and Richart Jr, 1984).

It is now common practice to use scaling laws when testing geotechnical structures such as slopes and retaining walls on a 1*g* shaking table (Yazdandoust, 2017; Xu P et al., 2020; Yünkül and Gürbüz, 2022). Based on the size of the model container and the capacity of the shaking table equipment, the geometric scale was chosen to be N=4 and the similarity ratio of acceleration and density to be 1.0. By considering the correction of the soil shear modulus, the similarity relationship is determined for the remaining physical quantities, as shown in Table 1.

2.3 Model geometry

A cantilever retaining wall with reinforced and unreinforced cohesionless backfill was subjected to two sets of shaking table tests, referred to in this study as the reinforced and unreinforced models. Fig. 2 illustrates the instrumentation arrangement and schematic

Table 1 Scaling laws used for the 1*g* shaking table test in this study

Parameter	Unit	Scaling factor (prototype/model)		Scaling factor used in this study (prototype/model)	
		(Iai, 1989)	(Wood, 2004)	(Iai, 1989)	(Wood, 2004)
Length, L	m	N	N	4	4
Acceleration, a	m/s^2	1	1	1	1
Density, ρ	kg/m^3	1	1	1	1
Shear modulus, G	kPa	N	N^{λ}	4	2
Stress, σ	kPa	N	N	4	4
Strain, ε		1	$N^{1-\lambda}$	1	2
Displacement, S	m	N	$N^{2-\lambda}$	4	8
Velocity, V	m/s	$N^{1/2}$	$N^{1-\lambda/2}$	2	2.83
Time, t	s	$N^{1/2}$	$N^{1-\lambda/2}$	2	2.83
Frequency, f	Hz	$N^{-1/2}$	$N^{-1+\lambda/2}$	0.5	0.35
Tensile strength, T	kN/m	N^2	N^2	16	16
Tensile stiffness, J	kN/m	N^2	N^2	16	16

N: geometric scale of prototype to physical model (prescribed as 4); λ: governing parameter in relation to soil type (assumed to be 0.5)

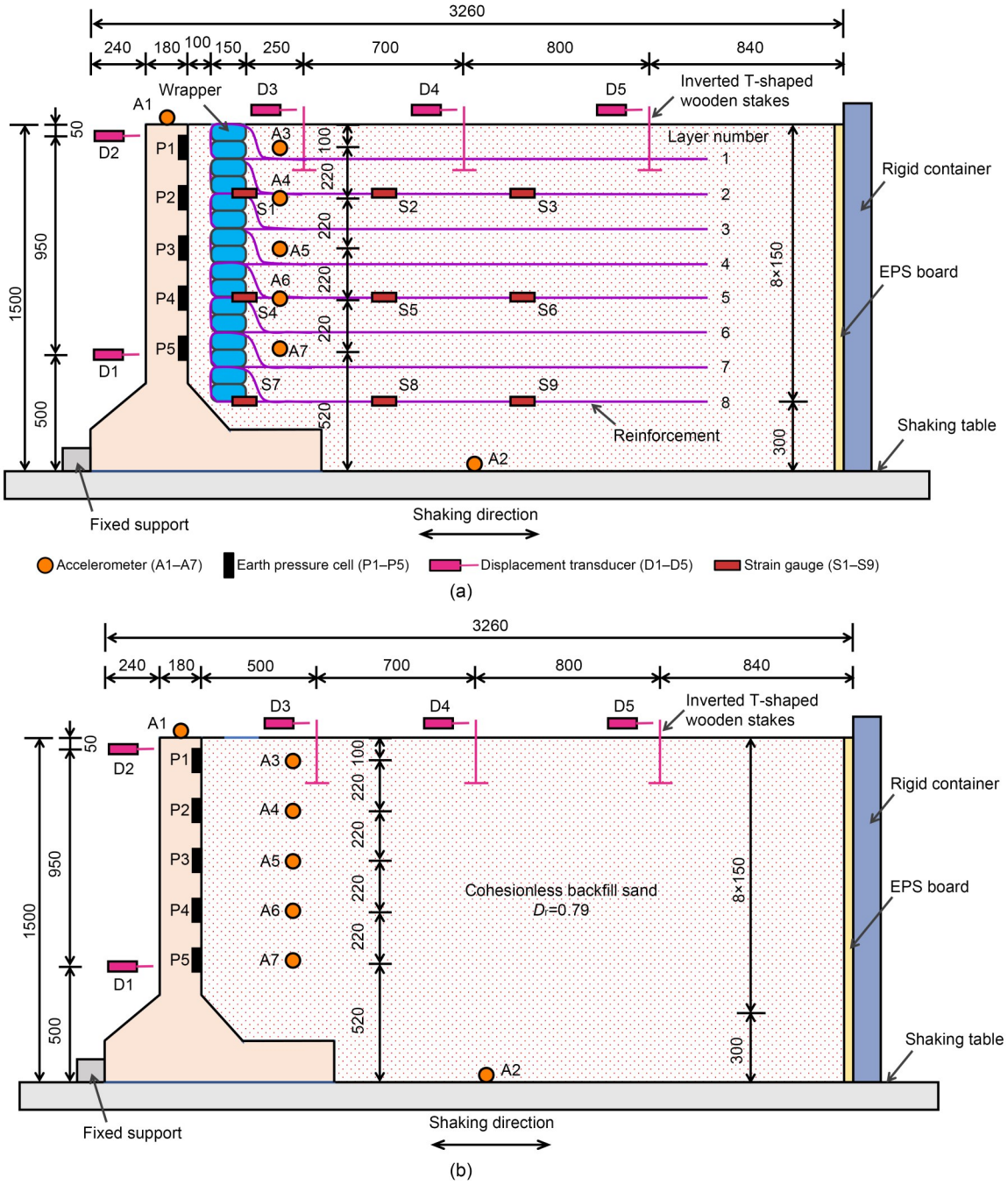

Fig. 2 Profile view of model configuration: (a) reinforced model; (b) unreinforced model (unit: mm). D_r is the relative density

geometry of the two sets of models. Both models have identical geometric dimensions, with a height of 1.50 m and a width of 3.26 m along the shaking direction. The backfill is of the same height as the retaining wall. An iron platen was used on the shaking table to support the model retaining wall, and the foundation was considered a stiff, rigid foundation, as in another study (Nakajima et al., 2021). The toe restraint boundary profoundly affects the seismic behaviour of a retaining wall, whether it is hinged or sliding (El-Emam and Bathurst, 2005; Yünkül and Gürbüz, 2022). In the present study, the toe of the retaining structure is restricted from horizontal translation but allowed to rotate (in other words, there is a hinged toe boundary) for modelling the embedment depth in the two models. The reinforced backfill model uses eight

layers of reinforcement from bottom to top at a spacing of 0.15 m. The ratio of reinforcement length to wall height (L/H) was 1.23, which was out of the experience value range of reinforcement length of 0.8–1.0. Furthermore, between the wrapper and the stem of the retaining wall is a bedding layer of 0.1-m-thick coarse sand. Since the retaining wall is not symmetrical in the transverse direction of the road or rail lines, there are mainly two states in the wall–soil interaction: soil thrusting the wall and wall squeezing the soil. The soil thrusting the wall represents the most unfavourable scenario, which determines the direction of vibration applied.

2.4 Materials

Locally available air-dried river sand, primarily composed of quartz with a specific gravity of 2.63, was used as the backfill material. In terms of dry unit weights, the maximum and minimum are 18.7 and 13.3 kN/m^3, respectively. By the Unified Soil Classification System, the backfill material was classified as poorly graded sand with 2.87% fines, coefficient of curvature C_c=0.76, and coefficient of uniformity C_u= 7.81. Each model test was conducted with a bulk unit weight of 17.3 kN/m^3 (D_r=79%) and moisture content w=1%. Direct shear tests were conducted using the same vertical stress levels and bulk unit weight indicated in the model walls. The peak friction angle of the backfill was determined to be approximately 47.7°.

The prototype of the model is to be used for fill sections of high-speed rails in a high seismic hazard zone. The model retaining wall was scaled at a ratio of 1:4 to the prototype wall. The wall was made of precast C40 grade concrete. The model wall configurations were determined by both the loading capacity of the shaking table and the similitude in Table 1. To simulate the 6-m height of the prototype, the model retaining wall was designed to have a height of 1.5 m. Other dimensions of the model retaining wall were determined accordingly, producing a wall bottom width of 1.0 m, a cantilever stem width of 0.18 m, a wall heel slab thickness of 0.18 m, and a length of 1.45 m along the line alignment. The rebar reinforcement of the model retaining wall was scaled down correspondingly. The earth pressure cells were mounted in five concave cylindrical holes on the back of the model retaining wall. In addition, three hollow polyvinyl chloride (PVC) pipes were embedded when the model wall was fabricated, thereby making the fluid lines of earth pressure cell leading out of the wall chest. The relative flexibility was determined according to Veletsos and Younan (1997). The relative flexibility of the model wall-soil system is approximately 4.73 (prototype is 6.31), indicating that the model retaining wall was rigid (Ertugrul and Trandafir, 2013; Liu et al., 2021). The model and prototype are close enough in flexibility to meet similarity requirements, suggesting a good model design.

An essential step in the reinforced soil model test is selecting the reinforcement material. Based upon the similarity relationships in Table 1, it is often difficult for the prototype geogrid to satisfy the mechanical similarity. Researchers usually use phosphor-bronze strips to replace geogrid in 1g shaking table tests (Watanabe et al., 2003; Tatsuoka et al., 2009; Yazdandoust, 2017; Xu P et al., 2020). The reinforcement layers were simulated by welding phosphor-bronze strips with an aperture size of 0.3 m (longitudinal)×0.15 m (transverse) and 0.2 mm thick. The tensile strength and stiffness of the single-layer phosphor-bronze mesh were 11.2 and 1467 kN/m, respectively. Because the prototype reinforcement spacing is 30 cm, the spacing of reinforcements should be 7.5 cm if the geometric scaling is strictly applied, making the model filling process difficult. As a compromise, the vertical spacing of the reinforcement in the model was set at 15 cm. According to the scaling laws, the tensile strength and stiffness of the single-layer reinforcement correspond to 89.6 and 11736 kN/m for the prototype. The prototype reinforcement becomes a very stiff geogrid material (Hatami and Bathurst, 2000; Safaee et al., 2021). Foil strain gauges were attached to measure the tensile strain developed within the reinforcement on the second, fifth, and eighth layers. Fig. 3 illustrates the arrangement of reinforcement and strain gauges.

2.5 Instrumentation and model construction

The model test included four types of instruments: earth pressure cell, accelerometer, strain gauge, and displacement transducer, as depicted in Fig. 2. There were seven uniaxial accelerometers with a maximum range of 2g, an accuracy of 0.01g, and an output sensitivity of 1000 mV/g. The accelerometer (A2) on the container base was used to record the shaking table's input motion. The soil acceleration responses at

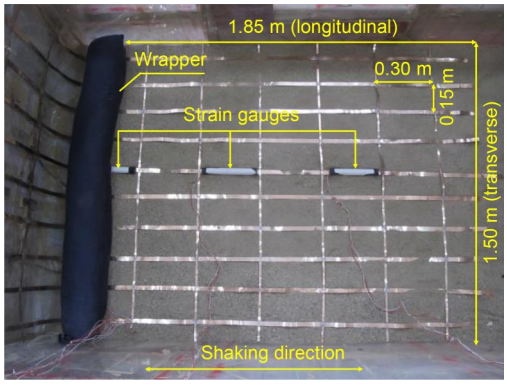

Fig. 3 Top view of the arrangement of model reinforcement and strain gauges

various elevations were monitored by embedding five accelerometers in the backfill (A3 to A7). Moreover, one accelerometer (A1) was installed on top of the cantilever wall to measure its acceleration response. All accelerometers detect motion parallel to the direction of shaking. Double-membrane earth pressure cells (67 mm in diameter), capable of measuring earth pressure up to 100 kPa with a resolution of 0.08 kPa, were installed in five predetermined cylindrical hollows at varying heights behind the retaining wall. We used five displacement transducers to measure the horizontal displacement response of the backfill and retaining wall. The retaining wall panel was measured at two points, near the toe and the top of the wall. Three additional displacement measurements were made in the backfill, at a distance of 0.5, 1.2, and 2.0 m from the back of the retaining wall. A wooden stake, buried inverted and T-shaped, was used to measure the horizontal displacements of the backfill surface. Due to the small displacement at the wall toe, an eddy current displacement sensor with a full range of 5 mm and an accuracy of 0.05 mm was utilized. By contrast, linear variable differential transducers with a measuring range of 10 cm and an accuracy of 0.5 mm were used for other measuring locations with larger displacement. In the reinforced model, nine strain measurement points were located on the surface of the phosphor-bronze strip. Half-bridge circuits were used to connect the strain gauges with a sensitivity factor of 2.15±0.02 and a resistance of 120 Ω, explicitly positioned on the second, fifth, and eighth layers of the central reinforcement strips. Note that waterproof treatment is required for all instrumentation.

All the sensors were connected to two high-frequency sensor data acquisition systems, each with 32 channels to collect synchronized simultaneous data. A sampling rate of 100 Hz was used in the test, and initial readings were set to zero before each excitation. Before filling the container with sand, transparent cellophane was pasted inside the acrylic glass to minimize boundary friction and ensure that the model exhibited in-plane strain. The prefabricated cantilever retaining wall was lifted into the model container and placed in a predetermined position. The gap between the retaining wall and the Plexiglas sidewall was filled with EPS sheets to prevent backfill sand from escaping. The wall was fitted with earth pressure cells on the back. The height of model was 1.5 m, evenly divided into 10 layers. A volume-controlled technique was used to achieve the same relative density D_r=79% in all layers. Sand mass was calculated by relating relative density to the volume. After that, a rigid steel plate was used to compact the backfill manually.

It is vital to lay the reinforcement as part of the reinforced model. Initially, the reinforcement mesh was laid horizontally over the backfill, and the sandbag was positioned neatly at the foldback section of the reinforcement. Next, the reinforcement was folded back and wrapped around the sandbag, and the back of the wrapper was filled and compacted to the target elevation for the layered fill. Lastly, a 0.1-m-thick space between the wrapper and stem of the wall was filled with sand of the same density. The whole construction process involved filling the reinforced body and the coarse sand bedding layer by layer, while accelerometers were buried at predetermined locations throughout the construction phase. The displacement sensors were installed once the model was filled. Fig. 4 illustrates the backfill procedure for the reinforced model.

2.6 Input ground motions

The dominant frequency of earthquake motions is between 0.1 and 10.0 Hz (Varnier and Hatami, 2011), and a typical earthquake record lasts between 10 and 30 s. In this study, a 9-s harmonic wave with a predominant frequency of 5 Hz was chosen as the input ground motion for the physical modelling. According to the scaling laws in Table 1, the prototype is subject to a harmonic wave with a duration of 25.47 s and a predominant frequency of 1.77 Hz. It is then reasonable to choose the nominal frequency and duration of the sinusoidal wave. The typical time histories

and Fourier spectra of the sine wave used in the test are shown in Fig. 5. There is a ramped cycle at the beginning of every acceleration signal, 40 constant-amplitude cycles in the middle, and one ramped cycle at the end. This condition is coincident with the gradual increase, steadying, and gradual decay of natural earthquake records (Bathurst and Hatami, 1998; Xu P et al., 2020). The input motions are amplified to three levels of input peak base acceleration (PBA) of 0.11*g*, 0.24*g*, and 0.39*g*, corresponding to probabilities of

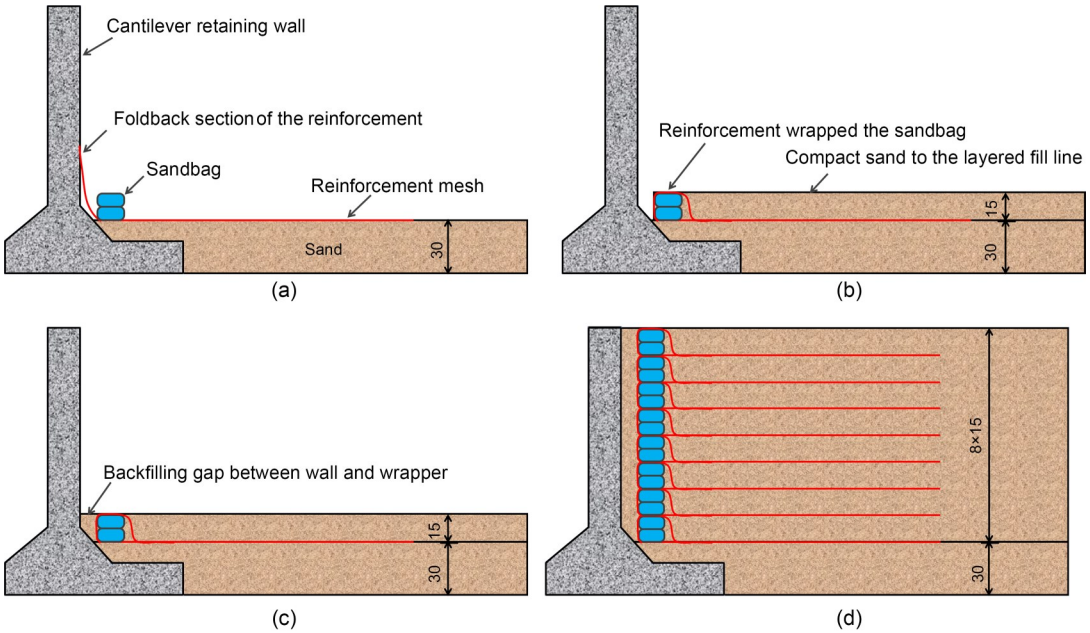

Fig. 4 Procedure of backfill in the reinforced model: (a) laying of reinforcement and stacking of sandbag; (b) reinforcement wrapped the sandbag; (c) backfilling the gap between wall and wrapper; (d) completion of the model construction (unit: cm)

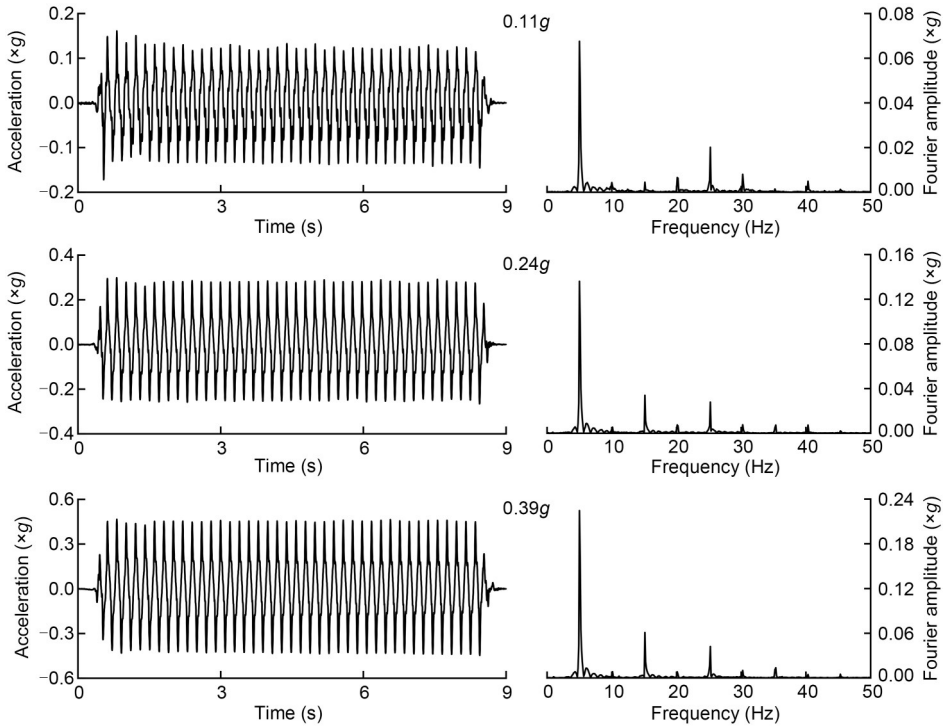

Fig. 5 Acceleration time histories and Fourier spectra of the input harmonic waves

exceedance in 50 years of 63%, 10%, and 2% for the prototype structure in a high seismic hazard zone, respectively. In this research, these three inputs are referred to as minor, moderate, and major earthquakes (Lu et al., 2018). Researchers have used sinusoidal waves as inputs to the shaking table test to investigate the dynamic response of retaining walls (Krishna and Latha, 2007; Safaee et al., 2021; Xu et al., 2021; Yünkül and Gürbüz, 2022). From Fig. 5, it is also evident that the sinusoidal signal is not perfectly harmonic, and contains the high-order harmonics of the integral times of the predominant frequency. This phenomenon is due to the nonlinear problem in the servo system of the electro-hydraulic shaking table. These high-order harmonics are part of the effect of the mechanical actions on the models (Brennan et al., 2005; Conti et al., 2012; Yao et al., 2014). Therefore, these high-order harmonics cannot be filtered out. A frequency sweep is used to detect changes in dynamic properties of the model after each stage of sinusoidal loading with white noise of 0.05g acceleration and a duration of 30 s.

3 Analysis and discussion

Before analyzing test results, it is crucial to first clarify the sign conventions for acceleration, displacement, earth pressure, and reinforcement load. When the value of input acceleration is assumed negative, the wall-soil system is subject to the seismic inertia force toward the free surface, moving away from the backfill relative to the shaking table. The displacement value is assumed positive to show the active state of the soil thrusting the wall, and vice versa. It is described below how each test quantity relates to the input acceleration when it is negative. The retaining wall and the backfill interact if the earth pressure is positive, and the backfill is unloading when the earth pressure is negative. Positive reinforcement load indicates that the reinforcement is in extension.

3.1 Fundamental frequency

Among the critical parameters in retaining wall dynamics is the fundamental frequency (Hatami and Bathurst, 2000). Analyzing the transfer function of the retaining wall model, which is defined as the ratio between the frequency content of the response to input motion, we determined the fundamental frequency. Upon input of the white noise signal to the shaking table, the acceleration time history of each acceleration measurement point is obtained. The transfer function TF(f, j) at a given frequency f and measurement point j is defined by

$$\mathrm{TF}(f,j)=\frac{P_{\mathrm{oi}}(f,j)}{P_{\mathrm{ii}}(f)}, \tag{1}$$

where $P_{\mathrm{oi}}(f,j)$ is the cross-power spectral of measurement point j and shaking table input signal, $P_{\mathrm{ii}}(f)$ is the self-power spectral of the input signal (Brennan and Madabhushi, 2009; Krishna and Bhattacharjee, 2017). Fig. 6 depicts the transfer function results at different monitoring points for the reinforced and unreinforced models once the construction is complete. As can be seen, the first fundamental frequencies of each measuring point are nearly equal. The fundamental frequencies of the unreinforced and reinforced models are comparable (22.71 and 22.69 Hz). Because of this, the effect of backfill reinforcement on cantilevered retaining walls before earthquakes is minimal. Based on the scaling law for the frequency in Table 1, the fundamental frequencies of the unreinforced and reinforced prototype structures are 7.95 and 7.94 Hz, respectively, which are in the range of medium-high frequency earthquakes. The fundamental frequency is mainly affected by the input ground motion intensity

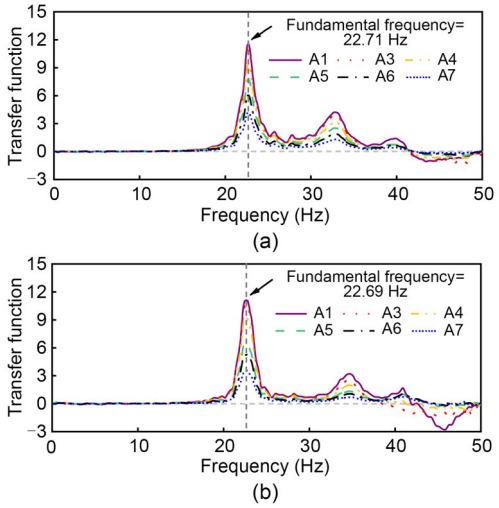

Fig. 6 Transfer function of six locations to base accelerations in unreinforced and reinforced models: (a) unreinforced model; (b) reinforced model

and the ratio of width to height for backfill. At the same time, the effect of reinforcement length and stiffness is less significant (Hatami and Bathurst, 2000).

Fig. 7 illustrates the fundamental frequencies of two models following earthquakes of varying intensities. It is evident that with the increase in loading amplitude, the fundamental frequency exhibits a monotonic decline, and the model structure gradually experiences degeneration, which is as expected. The fundamental frequencies of the unreinforced and reinforced models are similar after 0.11*g* loading, while they differ after 0.24*g* and 0.39*g* loadings. A lower value for the unreinforced model than that for its counterpart suggests that the reinforcement mitigates the stiffness degradation and potential structural damage.

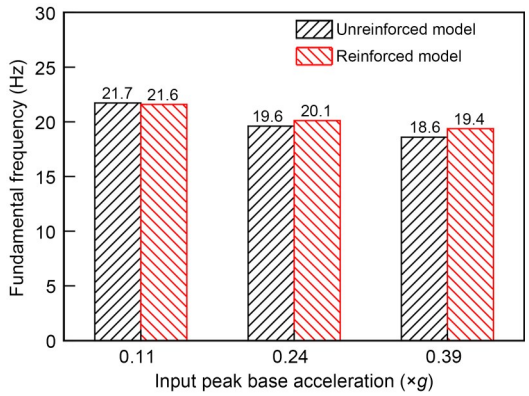

Fig. 7 Fundamental frequencies of unreinforced and reinforced models versus different input peak base accelerations

3.2 Acceleration

Acceleration response is another essential indicator of the seismic performance of geotechnical structures. Fig. 8 shows the acceleration time histories of the unreinforced model and its Fourier spectrum under 0.39*g* loading. The duration of the time history is limited to 1 s in order to avoid ambiguity. One can see that there is a delay between the acceleration response and the input signal; the negative peak of measurement point *j* is delayed by $\Delta t(j)$ when the acceleration peaks in the negative direction. Besides, the acceleration peak increases with the elevation of the measurement point, and the curve gradually becomes more irregular, suggesting an increase in the high-frequency component. Fourier analysis corroborates this by showing that amplification occurs not only at the 5-Hz domain frequency, but also at the higher-order harmonics.

The phase shift between the input ground motion and acceleration measurement point *j* can be computed as

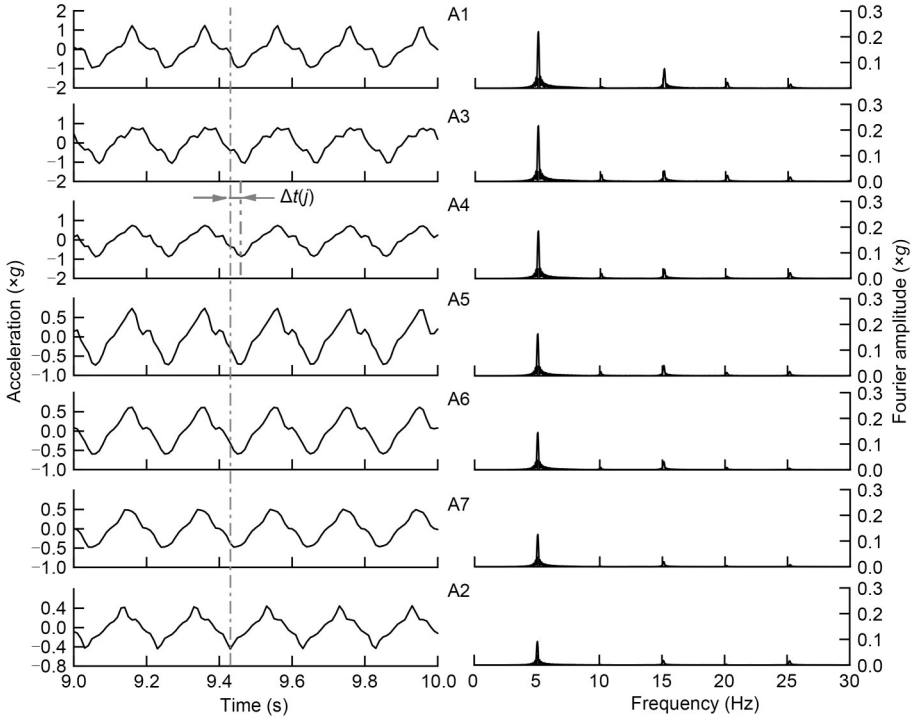

Fig. 8 Acceleration time histories and Fourier spectrum of the unreinforced model under 0.39*g* loading

$$\Delta\varphi(j)=f\Delta t(j)\times 360°, \tag{2}$$

where f denotes the predominant frequency of the input signal, and $\Delta t(j)$ denotes the propagation time of the wave from the shaking table to the measurement point j. The phase delay of the acceleration response at measurement points relative to the table is calculated and presented in Table 2. The phase shift increases as the height of the measurement point position increases, which is due to the time taken for the vibration wave to propagate from the table to each measurement point. The phase delay at the crest of the wall is slightly greater than that over the backfill surface for a smaller amplitude of input ground motion, while the opposite pattern occurs for major earthquakes. The phase delay of acceleration propagation in the model structure is not significant, whether reinforcement is provided or not.

Table 2 Phase delay between the response acceleration and input acceleration in time histories

Measurement point	Phase delay in unreinforced model (°)			Phase delay in reinforced model (°)		
	0.11*g*	0.24*g*	0.39*g*	0.11*g*	0.24*g*	0.39*g*
A1	54	54	36	36	54	36
A3	36	54	72	36	72	72
A4	36	54	54	36	54	54
A5	36	54	36	36	54	54
A6	18	36	36	36	36	36
A7	18	0	18	18	18	18

The amplification factor of root-mean-square acceleration (RMSA) evaluates the amplification and de-amplification effect at different elevations of the input ground motions. The RMSA can take into account the effects of amplitude and spectrum to reduce high-frequency signal noise, calculated by Kramer (1996).

$$\mathrm{RMSA}=\left[\frac{\frac{1}{t_\mathrm{d}}\int_0^{t_\mathrm{d}}a^2(t)\,\mathrm{d}t}{\frac{1}{t_\mathrm{d}}\int_0^{t_\mathrm{d}}b^2(t)\,\mathrm{d}t}\right]^{\frac{1}{2}}, \tag{3}$$

where t denotes the time, $a(t)$ is the time history of acceleration at different elevations, $b(t)$ is the acceleration time history of the input ground motion, and t_d is the duration of the acceleration record.

The distribution of acceleration amplification factors along the normalized height for the unreinforced and reinforced models is shown in Fig. 9. The normalized height is defined as the ratio of elevation of measurement points to the wall height. In both unreinforced and reinforced models, the acceleration amplification factor increases nonlinearly with the height of the wall; the acceleration at the crest of the wall is slightly greater than that on the backfill surface. However, in the traditional pseudo-static approaches or design codes, the acceleration is generally assumed to be uniform with increasing wall height. Increasing acceleration amplitude leads to an increase in acceleration amplification factor, possibly due to the strong boundary constraints of the retaining wall model. There is no evidence of particularly severe damage to the model, which is well maintained within the tested amplitude range. An unreinforced model has a smaller acceleration amplification factor as a reinforced model, indicating that the soil with reinforcement can effectively mitigate the amplification effect of ground shaking. At 0.11*g*, the acceleration amplification factors of both models are similar, indicating that the load amplitude has not yet reached the threshold acceleration required to mobilize the reinforcement effect (Ding et al., 2020). Under 0.24*g* and 0.39*g* loadings, the acceleration amplification factor of the reinforced model is significantly smaller than that of the unreinforced model by a reduction of 7.5%–11.7% and 3.7%–10.2%, respectively.

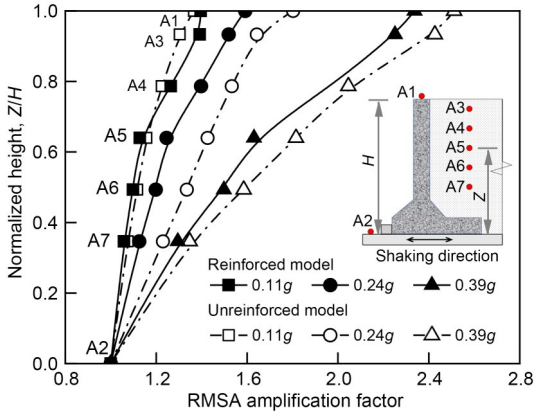

Fig. 9 Distribution of the acceleration amplification factor against the normalized height

3.3 Displacement

Fig. 10 shows the time histories of the acceleration at the base and top of the wall, the horizontal displacement, and the backfill. Displacement time

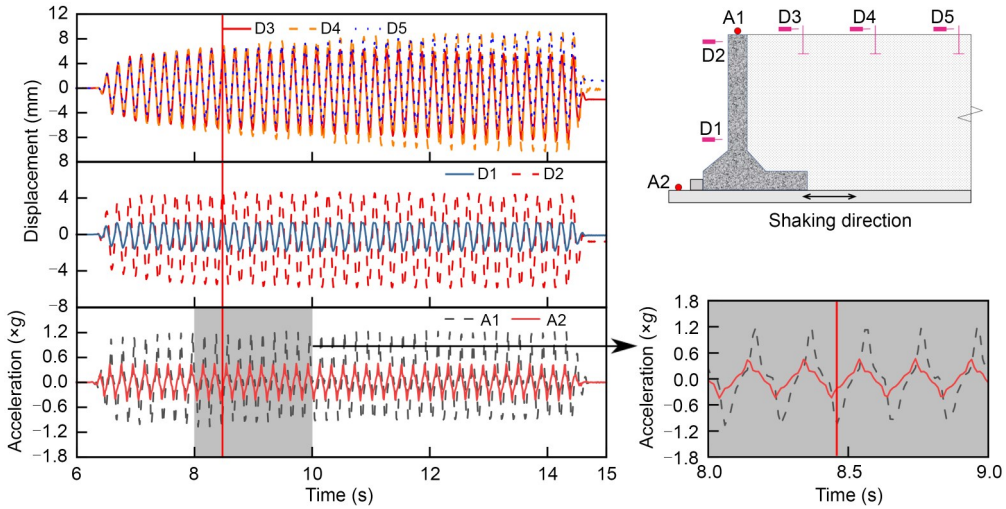

Fig. 10 Time histories of displacement and acceleration of the unreinforced model under 0.39*g* loading

histories follow a pattern consistent with the input motion, which is a harmonic wave. Since there is a phase difference between the input acceleration and the acceleration at the crest of the wall, we evaluated the dynamic response of each sensor at the moment when the wall acceleration obtains a negative peak, as opposed to when the input motion attains a negative peak. The wall is subject to the maximum seismic inertia force at this time. Therefore, the displacement measurement points are almost simultaneously reaching the positive peak. The soil thrusts the wall to the limit, putting its stability into the most unfavourable state. As residual displacement is small after the end of an earthquake, the peak displacement during the wall–soil interaction is the primary consideration.

Fig. 11 shows the peak horizontal displacement of the wall for the unreinforced and reinforced models. The displacement measurement points of the lower and upper portions of the wall are indicated by D1 and D2, respectively. Since the wall is rigid as a whole, the D1 and D2 displacement data have been connected and extended to intersect the coordinate axes. The displacement extension lines of all loading conditions converge at the origin; then the wall displacement mode is identified as rotating around the toe of the wall, which creates a good hinged restraint effect. The wall displacements increased with increasing load amplitude for both physical models. The reinforcement can reduce rotational displacement of the cantilever retaining wall in general. There is no apparent effect of backfill reinforcement on wall displacement under 0.11*g* loading. Under 0.24*g* loading, the wall rotation angles

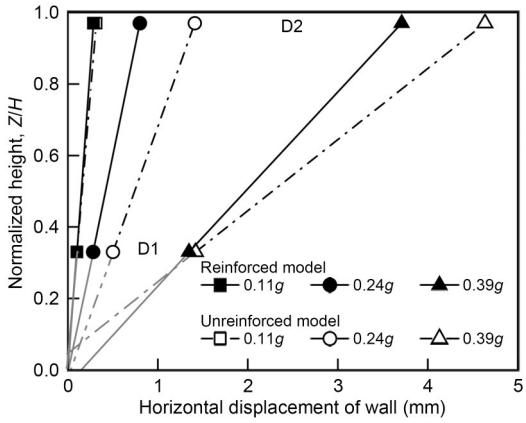

Fig. 11 Peak horizontal displacement of the wall during vibration

of the unreinforced and reinforced models are 0.96‰ and 0.55‰, respectively, producing a 43% reduction. Under 0.39*g* loading, the wall rotation angles were 3.39‰ and 2.49‰, respectively (27% reduction). Due to the improved soil strength and the reduced dynamic earth pressure, the soil reinforcement decreases the displacement of the retaining wall.

Additionally, three displacement measurement points were located on the surface of the backfill. The monitoring data show that backfill reinforcement also reduces the peak vibration displacement on the surface. The reinforcement effect is not apparent under the action of 0.11*g* loading. Under moderate and major earthquakes, the average displacement of the backfill surface was reduced by 22% and 20%, respectively. During a major earthquake, the rigid cantilever plate restrains the displacement of the backfill, and the

relative movement between the reinforcement and soil is small, mitigating the reinforcing effect of the backfill. It is recommended to reserve deformation conditions to maximize the effect of backfill reinforcement.

3.4 Earth pressure

A duration of 1 s is selected at each level during loading to investigate the wall–soil interaction law. Fig. 12 depicts the time histories of the acceleration a of A1 at the top of the wall, the dynamic earth pressures p of P1–P5 at the back of the wall, and the resultant force F of the dynamic earth pressure. The effect of reinforcement on the wall–soil interaction is observed. When the acceleration A1 reaches a negative peak value in the unreinforced model, the wall experiences a peak inertia force toward the free surface; the resultant force of dynamic earth pressure is then at its maximum, and earth pressure and inertia force are synchronized. Thus, the inertia force and seismic earth pressure are always synchronized, regardless of the load amplitude. As for the reinforced model, the synchronization of wall–soil interaction varies with the load amplitude. In 0.11g and 0.24g conditions, the resultant force is not at the positive peak but approximates zero when the wall acceleration is at negative peaks. This phenomenon implies no synchronized increase occurs for earth pressures measured at each location. The inertial force and seismic earth pressure synchronized again at 0.39g. In this case the seismic design of the retaining wall is based on the simultaneous maximum of the inertia force and the seismic earth pressure; an overly conservative design is thus obtained, which fails to reflect the actual wall–soil interaction under minor and moderate earthquakes. The phenomenon of wall–soil interaction asynchrony has been reported in the literature (Al Atik and Sitar, 2010; Jo et al., 2017). For low intensity earthquakes, the inertia force contributes significantly to the stability of the retaining wall; in contrast, the dynamic earth pressure acting on the wall back is significant at large earthquake intensity.

The distribution of dynamic earth pressure along the wall height under the unfavourable active state is shown in Fig. 13. The dynamic earth pressure distributions of the pseudo-static MO and SW methods are also given under 0.39g loading. The dynamic earth pressure is large at the top but decreases towards the bottom, consistent with the SW method. The measured earth pressure fluctuates around zero during minor and moderate earthquakes, and some measurement points even produce negative values, indicating the existence of unloading. Almost all dynamic soil pressure measurement points are reduced after backfill reinforcement; a few exceptions may be due to accidental error, but the dynamic earth pressure is generally reduced. The effect of backfill reinforcement on the distribution pattern of dynamic earth pressure is not apparent.

Fig. 14 shows the measured resultant forces of dynamic earth pressure of unreinforced and reinforced models. At the same time, the calculated values of the classical pseudo-static MO and SW methods are plotted. It can be seen that the backfill reinforcement reduces the resultant force at different load amplitudes. During minor and moderate earthquakes, the resultant force of the reinforced model is approximately zero because of the phase shift in wall–soil interactions. Although the wall–soil interaction is synchronized in a major earthquake, the reinforcement enhances the backfill integrity and reduces the resultant force by 18.3%. As the peak acceleration of the base increases, the resultant forces of both models increase nonlinearly. In both the minor and moderate earthquake cases, the measured resultant forces are smaller than the calculations by the MO and SW pseudo-static methods. However, in a major earthquake, the measured resultant forces are higher, consistent with previous study (Green et al., 2008). This phenomenon may be due to the attenuation of soil shear strength under high-intensity shaking loads (Koseki et al., 1998a).

3.5 Reinforcement load

The measured peak tensile force distribution in three reinforcement layers for the reinforced model is shown in Fig. 15, where the force is assumed to be zero at the free end of each reinforcement layer. The dynamic tensile load of the reinforcements is distributed non-uniformly and, with increasing reinforcement height, the maximum value is gradually displaced from the back of the wall. The dynamic tensile load of each measurement point increases at a larger load amplitude. Once the maximum values along the length of the reinforcement at different layers are connected, we can sketch the approximate location and shape of the potential failure surface of the backfill behind the wall. A piecewise polyline over the heel point of the

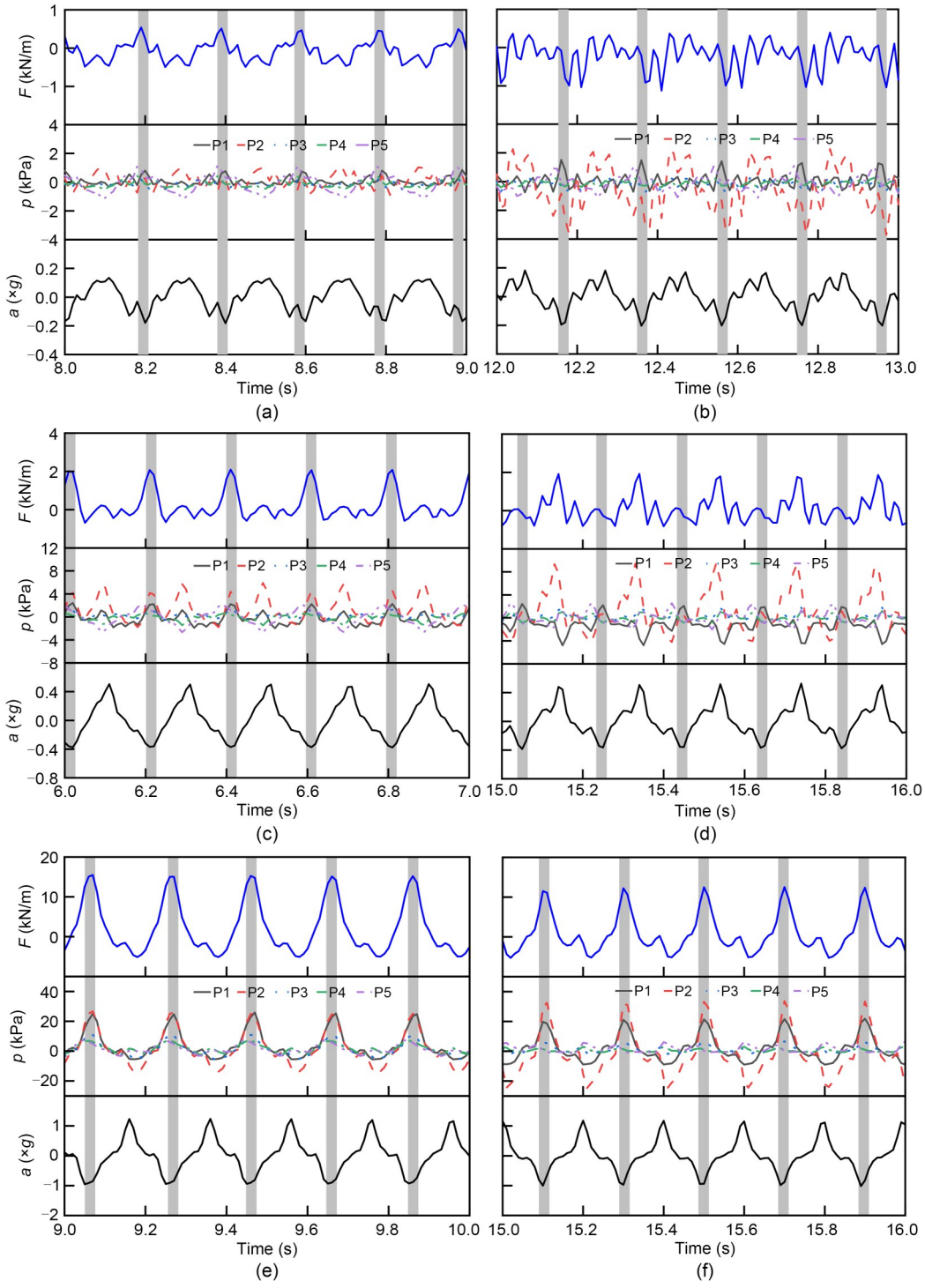

Fig. 12 Time histories of wall acceleration *a*, dynamic earth pressures *p*, and the resultant force *F*: (a) 0.11*g*-unreinforced model; (b) 0.11*g*-reinforced model; (c) 0.24*g*-unreinforced model; (d) 0.24*g*-reinforced model; (e) 0.39*g*-unreinforced model; (f) 0.39*g*-reinforced model

wall is approximated, with the upper half of the polyline being vertical and the lower half being curved. In the horizontal direction, the upper half vertical surface is approximately 0.58 times the wall height from the imaginary wall back passing through the heel point of the wall.

Fig. 16a plots the reinforcement load distribution along the height of three measurement points in the

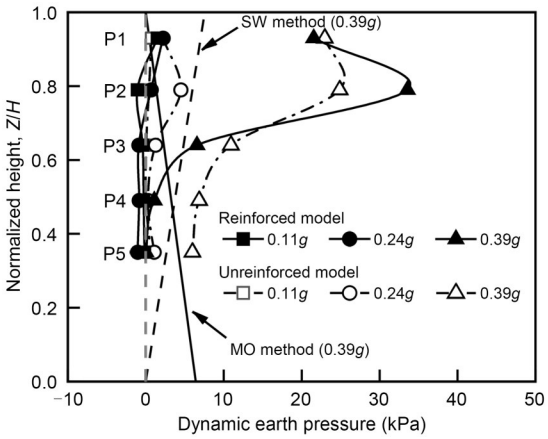

Fig. 13 Distribution of dynamic earth pressure along with the height of the wall at active state

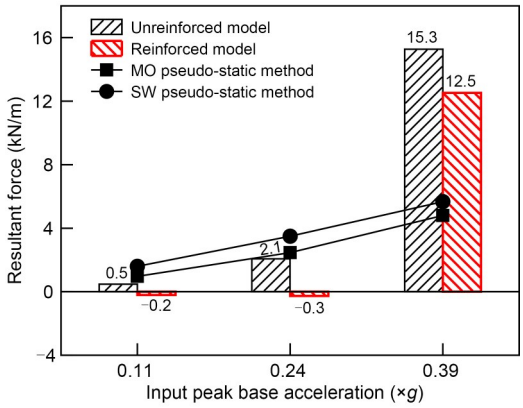

Fig. 14 Comparison of the experimental resultant forces of dynamic earth pressure with the calculations by the pseudo-static methods

direction of the reinforcement length. Also, the average tensile forces of nine measurement points during each loading were calculated to represent the dynamic response of the whole model, as shown in Fig. 16b. At 0.11*g*, the dynamic reinforcement load was small with an uniform distribution along the height; at 0.24*g*, the dynamic load increased to some extent as the reinforcement effect improved, and the distribution pattern was not significantly different with respect to the height; at 0.39*g*, the reinforcement load increased more significantly due to the prominent reinforcement effect, and the distribution pattern can be characterized as "large at both ends but small in the middle portion." Fig. 16b shows that loads on reinforcements are nonlinearly related to base acceleration.

4 Conclusions

An investigation of the seismic dynamics of cantilever retaining walls backfilled with reinforced and unreinforced soils was undertaken using 1/4 scale shaking table tests. The following are several observations from the experimental results:

1. Both models show a decrease in fundamental frequency with increasing input acceleration, and there is a degradation in stiffness and potential damage to the wall-soil system. The reinforced model reduces its fundamental frequency more than in the unreinforced model, indicating that reinforcing the backfill can

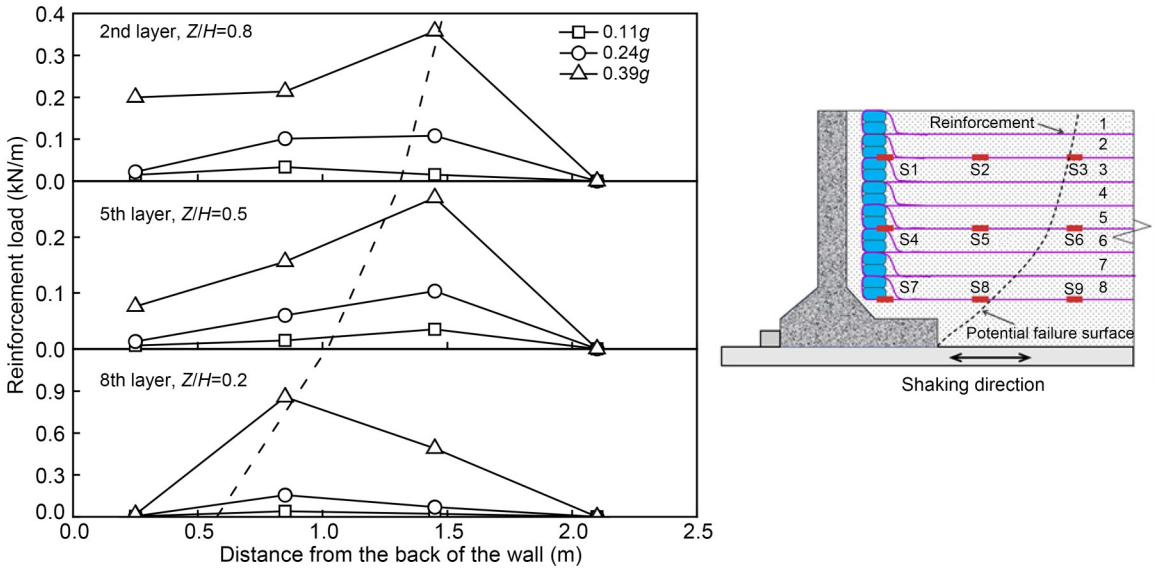

Fig. 15 Distribution of peak dynamic load in the reinforcement layer

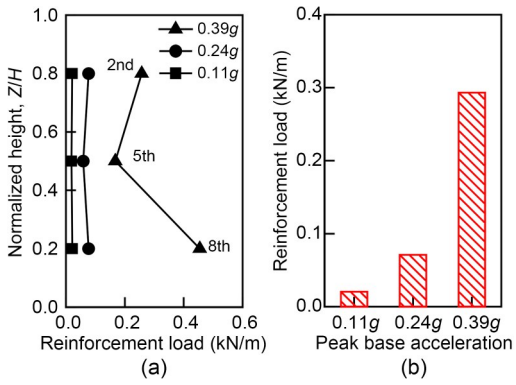

Fig. 16 Variation of reinforcement load with the height (a) and the load amplitude (b)

enhance the integrity of the wall-soil system and reduce seismic damage.

2. Based on RMSA, the amplification factor increases nonlinearly with increasing height, reaching its maximum at the top of the wall. However, design codes or pseudo-static approaches assume that the acceleration amplification factor stays constant throughout the height of the wall. A smaller acceleration amplification factor for the reinforced model than for the unreinforced one indicates that backfill reinforcement can mitigate the amplification effect of the input motion.

3. The seismic displacement of cantilever retaining walls increases nonlinearly at larger load amplitudes. Reinforcement has a restraining effect on wall/soil displacement that depends on the input acceleration. The capacity of backfill reinforcement to restrain displacement is constrained by the phenomenon of "backfill chasing the wall" at 0.39*g* loading.

4. During a period when the wall is subject to the greatest inertia force away from the backfill, the wall is considered most unstable. The inclusion of reinforcement yields a phase difference between the actions of the wall inertia force and the dynamic earth pressure under 0.11*g* and 0.24*g* loading. The wall inertia forces and dynamic earth pressures of both models were synchronized during 0.39*g* loading, but the resultant force in the reinforced model was still 18.3% less than that in the unreinforced one.

5. During seismic excitation, the reinforcement longitude exhibited a nonlinear dynamic tensile force and the reinforcement load distribution along the wall height did not follow a constant pattern. In an approximate failure surface, the upper half of a piecewise polyline is vertical and the lower half is curved over the heel. The measured dynamic tensile force increased nonlinearly at a larger input acceleration amplitude.

Differential movement between soil and reinforcement greatly affects the reinforced backfill effect on the structure's seismic performance. Future research should consider more technical measures to enhance the differential movement and to explore its role in improving seismic performance of retaining structures in major earthquakes.

Acknowledgments

This work is supported by the National Natural Science Foundation of China (Nos. 41901073 and 52078435) and the Sichuan Science and Technology Program of China (No. 2021YJ0001).

Author contributions

Qiang LUO designed the research. Ming WEI and Gui-shuai FENG processed the corresponding data. Ming WEI wrote the first draft of the manuscript. Liang-wei JIANG helped to organize the manuscript. Teng-fei WANG revised and edited the final version.

Conflict of interest

Ming WEI, Qiang LUO, Gui-shuai FENG, Teng-fei WANG, and Liang-wei JIANG declare that they have no conflict of interest.

References

Al Atik L, Sitar N, 2010. Seismic earth pressures on cantilever retaining structures. *Journal of Geotechnical and Geoenvironmental Engineering*, 136(10):1324-1333. https://doi.org/10.1061/(ASCE)GT.1943-5606.0000351

Bathurst RJ, Hatami K, 1998. Seismic response analysis of a geosynthetic-reinforced soil retaining wall. *Geosynthetics International*, 5(1-2):127-166. https://doi.org/10.1680/gein.5.0117

Brennan AJ, Madabhushi SPG, 2009. Amplification of seismic accelerations at slope crests. *Canadian Geotechnical Journal*, 46(5):585-594. https://doi.org/10.1139/T09-006

Brennan AJ, Thusyanthan NI, Madabhushi SP, 2005. Evaluation of shear modulus and damping in dynamic centrifuge tests. *Journal of Geotechnical and Geoenvironmental Engineering*, 131(12):1488-1497. https://doi.org/10.1061/(ASCE)1090-0241(2005)131:12(1488)

Conti R, Madabhushi GSP, Viggiani GMB, 2012. On the behaviour of flexible retaining walls under seismic actions. *Géotechnique*, 62(12):1081-1094. https://doi.org/10.1680/geot.11.P.029

Ding GY, Zhou L, Wang J, et al., 2020. Shaking table tests on gravel slopes reinforced by concrete canvas. *Geotextiles and Geomembranes*, 48(4):539-545.

https://doi.org/10.1016/j.geotexmem.2020.02.012

Edinçliler A, Toksoy YS, 2017. Physical model study of the seismic performance of highway embankments with and without geotextile. *Journal of Earthquake and Tsunami*, 11(2):1750003. https://doi.org/10.1142/S1793431117500038

Eftekhari Z, Panah AK, 2021. 1-*g* shaking table investigation on seismic performance of polymeric-strip reinforced-soil retaining walls built on rock slopes with limited reinforced zone. *Soil Dynamics and Earthquake Engineering*, 147: 106758. https://doi.org/10.1016/j.soildyn.2021.106758

El-Emam MM, Bathurst RJ, 2005. Facing contribution to seismic response of reduced-scale reinforced soil walls. *Geosynthetics International*, 12(5):215-238. https://doi.org/10.1680/gein.2005.12.5.215

El-Emam MM, Bathurst RJ, 2007. Influence of reinforcement parameters on the seismic response of reduced-scale reinforced soil retaining walls. *Geotextiles and Geomembranes*, 25(1):33-49. https://doi.org/10.1016/j.geotexmem.2006.09.001

Ertugrul OL, Trandafir AC, 2013. Lateral earth pressures on flexible cantilever retaining walls with deformable geofoam inclusions. *Engineering Geology*, 158:23-33. https://doi.org/10.1016/j.enggeo.2013.03.001

Ertugrul OL, Trandafir AC, Ozkan MY, 2017. Reduction of dynamic earth loads on flexible cantilever retaining walls by deformable geofoam panels. *Soil Dynamics and Earthquake Engineering*, 92:462-471. https://doi.org/10.1016/j.soildyn.2016.10.011

Gao HM, Hu Y, Wang ZH, et al., 2017. Shaking table tests on the seismic performance of a flexible wall retaining EPS composite soil. *Bulletin of Earthquake Engineering*, 15(12): 5481-5510. https://doi.org/10.1007/s10518-017-0189-4

Green RA, Olgun CG, Cameron WI, 2008. Response and modeling of cantilever retaining walls subjected to seismic motions. *Computer-Aided Civil and Infrastructure Engineering*, 23(4):309-322. https://doi.org/10.1111/j.1467-8667.2007.00538.x

Hardin BO, Drnevich VP, 1972. Shear modulus and damping in soils: design equations and curves. *Journal of the Soil Mechanics and Foundations Division*, 98(7):667-692. https://doi.org/10.1061/JSFEAQ.0001760

Hatami K, Bathurst RJ, 2000. Effect of structural design on fundamental frequency of reinforced-soil retaining walls. *Soil Dynamics and Earthquake Engineering*, 19(3):137-157. https://doi.org/10.1016/S0267-7261(00)00010-5

Huang CC, 2019. Seismic responses of vertical-faced wrap-around reinforced soil walls. *Geosynthetics International*, 26(2):146-163. https://doi.org/10.1680/jgein.18.00044

Iai S, 1989. Similitude for shaking table tests on soil-structure-fluid model in 1*g* gravitational field. *Soils and Foundations*, 29(1):105-118. https://doi.org/10.3208/sandf1972.29.105

Jo SB, Ha JG, Lee JS, et al., 2017. Evaluation of the seismic earth pressure for inverted T-shape stiff retaining wall in cohesionless soils via dynamic centrifuge. *Soil Dynamics and Earthquake Engineering*, 92:345-357. https://doi.org/10.1016/j.soildyn.2016.10.009

Kamiloğlu HA, Şadoğlu E, 2019. A method for active seismic earth thrusts of granular backfill acting on cantilever retaining walls. *Soils and Foundations*, 59(2):419-432. https://doi.org/10.1016/j.sandf.2018.12.003

Kilic IE, Cengiz C, Edincliler A, et al., 2021. Seismic behavior of geosynthetic-reinforced retaining walls backfilled with cohesive soil. *Geotextiles and Geomembranes*, 49(5):1256-1269. https://doi.org/10.1016/j.geotexmem.2021.04.004

Kokusho T, 1980. Cyclic triaxial test of dynamic soil properties for wide strain range. *Soils and Foundations*, 20(2): 45-60. https://doi.org/10.3208/sandf1972.20.2_45

Koseki J, Tatsuoka F, Munaf Y, et al., 1998a. A modified procedure to evaluate active earth pressure at high seismic loads. *Soils and Foundations*, 38(S1):209-216. https://doi.org/10.3208/sandf.38.Special_209

Koseki J, Munaf Y, Tatsuoka F, et al., 1998b. Shaking and tilt table tests of geosynthetic-reinforced soil and conventional-type retaining walls. *Geosynthetics International*, 5(1-2): 73-96. https://doi.org/10.1680/gein.5.0115

Kramer SL, 1996. Geotechnical Earthquake Engineering. Pearson, Upper Saddle River, USA, p.65-83.

Krishna AM, Latha GM, 2007. Seismic response of wrap-faced reinforced soil-retaining wall models using shaking table tests. *Geosynthetics International*, 14(6):355-364. https://doi.org/10.1680/gein.2007.14.6.355

Krishna AM, Latha GM, 2009. Seismic behaviour of rigid-faced reinforced soil retaining wall models: reinforcement effect. *Geosynthetics International*, 16(5):364-373. https://doi.org/10.1680/gein.2009.16.5.364

Krishna AM, Bhattacharjee A, 2017. Behavior of rigid-faced reinforced soil-retaining walls subjected to different earthquake ground motions. *International Journal of Geomechanics*, 17(1):06016007. https://doi.org/10.1061/(asce)gm.1943-5622.0000668

Li SH, Cai XG, Jing LP, et al., 2021. Lateral displacement control of modular-block reinforced soil retaining walls under horizontal seismic loading. *Soil Dynamics and Earthquake Engineering*, 141:106485. https://doi.org/10.1016/j.soildyn.2020.106485

Liu H, Han J, Parsons RL, 2021. Mitigation of seasonal temperature change-induced problems with integral bridge abutments using EPS foam and geogrid. *Geotextiles and Geomembranes*, 49(5):1380-1392. https://doi.org/10.1016/j.geotexmem.2021.05.010

Lu XL, Chen C, Jiang HJ, et al., 2018. Shaking table tests and numerical analyses of an RC coupled wall structure with replaceable coupling beams. *Earthquake Engineering & Structural Dynamics*, 47(9):1882-1904. https://doi.org/10.1002/eqe.3046

Mononobe N, Matsuo H, 1929. On the determination of earth pressure during earthquakes. Proceedings of the World

Engineering Conference, p.177-185.

Nakajima S, Ozaki T, Sanagawa T, 2021. 1*g* shaking table model tests on seismic active earth pressure acting on retaining wall with cohesive backfill soil. *Soils and Foundations*, 61(5):1251-1272. https://doi.org/10.1016/j.sandf.2021.06.014

Osouli A, Zamiran S, 2017. The effect of backfill cohesion on seismic response of cantilever retaining walls using fully dynamic analysis. *Computers and Geotechnics*, 89:143-152. https://doi.org/10.1016/j.compgeo.2017.04.007

Ren FF, Huang QQ, Wang G, 2020. Shaking table tests on reinforced soil retaining walls subjected to the combined effects of rainfall and earthquakes. *Engineering Geology*, 267:105475. https://doi.org/10.1016/j.enggeo.2020.105475

Safaee AM, Mahboubi A, Noorzad A, 2021. Experimental investigation on the performance of multi-tiered geogrid mechanically stabilized earth (MSE) walls with wrap-around facing subjected to earthquake loading. *Geotextiles and Geomembranes*, 49(1):130-145. https://doi.org/10.1016/j.geotexmem.2020.08.008

Samee AA, Yazdandoust M, Ghalandarzadeh A, 2022. Effect of reinforcement arrangement on dynamic behaviour of back-to-back mechanically stabilised earth walls. *International Journal of Physical Modelling in Geotechnics*, 22(4):208-223. https://doi.org/10.1680/jphmg.20.00088

Seed HB, Whitman RV, 1970. Design of earth retaining structures for dynamic loads. Proceedings of the ASCE Specialty Conference on Lateral Stresses in the Ground and Design of Earth Retaining Structures, p.103-147.

Tatsuoka F, Tateyama M, Koseki J, 1996. Performance of soil retaining walls for railway embankments. *Soils and Foundations*, 36(S1):311-324. https://doi.org/10.3208/sandf.36.Special_311

Tatsuoka F, Tateyama M, Mohri Y, et al., 2007. Remedial treatment of soil structures using geosynthetic-reinforcing technology. *Geotextiles and Geomembranes*, 25(4-5):204-220. https://doi.org/10.1016/j.geotexmem.2007.02.002

Tatsuoka F, Hirakawa D, Nojiri M, et al., 2009. A new type of integral bridge comprising geosynthetic-reinforced soil walls. *Geosynthetics International*, 16(4):301-326. https://doi.org/10.1680/gein.2009.16.4.301

Varnier JB, Hatami K, 2011. Seismic response of reinforced soil retaining walls: is PGA-based design adequate? Georisk 2011, p.336-343. https://doi.org/doi:10.1061/41183(418)28

Veletsos AS, Younan AH, 1997. Dynamic response of cantilever retaining walls. *Journal of Geotechnical and Geoenvironmental Engineering*, 123(2):161-172. https://doi.org/10.1061/(ASCE)1090-0241(1997)123:2(161)

Wang LY, Chen GX, Chen S, 2015. Experimental study on seismic response of geogrid reinforced rigid retaining walls with saturated backfill sand. *Geotextiles and Geomembranes*, 43(1):35-45. https://doi.org/10.1016/j.geotexmem.2014.11.006

Watanabe K, Munaf Y, Koseki J, et al., 2003. Behaviors of several types of model retaining walls subjected to irregular excitation. *Soils and Foundations*, 43(5):13-27. https://doi.org/10.3208/sandf.43.5_13

Watanabe K, Nakajima S, Fujii K, et al., 2020. Development of geosynthetic-reinforced soil embankment resistant to severe earthquakes and prolonged overflows due to tsunamis. *Soils and Foundations*, 60(6):1371-1386. https://doi.org/10.1016/j.sandf.2020.08.006

Wilson P, Elgamal A, 2015. Shake table lateral earth pressure testing with dense *c*-ϕ backfill. *Soil Dynamics and Earthquake Engineering*, 71:13-26. https://doi.org/10.1016/j.soildyn.2014.12.009

Wood DM, 2004. Geotechnical Modelling. CRC Press, London, UK, p.233-258.

Wood DM, Crewe A, Taylor C, 2002. Shaking table testing of geotechnical models. *International Journal of Physical Modelling in Geotechnics*, 2(1):1-13. https://doi.org/10.1680/ijpmg.2002.020101

Xu C, Luo MM, Shen PP, et al., 2020. Seismic performance of a whole geosynthetic reinforced soil-integrated bridge system (GRS-IBS) in shaking table test. *Geotextiles and Geomembranes*, 48(3):315-330. https://doi.org/10.1016/j.geotexmem.2019.12.004

Xu P, Hatami K, Jiang GL, 2020. Study on seismic stability and performance of reinforced soil walls using shaking table tests. *Geotextiles and Geomembranes*, 48(1):82-97. https://doi.org/10.1016/j.geotexmem.2019.103507

Xu P, Hatami K, Jiang GL, 2021. Shaking table performance of reinforced soil retaining walls with different facing configurations. *Geotextiles and Geomembranes*, 49(3):516-527. https://doi.org/10.1016/j.geotexmem.2020.10.003

Yao JJ, Di DT, Jiang GL, et al., 2014. Real-time acceleration harmonics estimation for an electro-hydraulic servo shaking table using Kalman filter with a linear model. *IEEE Transactions on Control Systems Technology*, 22(2):794-800. https://doi.org/10.1109/tcst.2013.2256136

Yazdandoust M, 2017. Investigation on the seismic performance of steel-strip reinforced-soil retaining walls using shaking table test. *Soil Dynamics and Earthquake Engineering*, 97:216-232. https://doi.org/10.1016/j.soildyn.2017.03.011

Yu PJ, Richart Jr FE, 1984. Stress ratio effects on shear modulus of dry sands. *Journal of Geotechnical Engineering*, 110(3):331-345. https://doi.org/10.1061/(ASCE)0733-9410(1984)110:3(331)

Yünkül K, Gürbüz A, 2022. Shaking table study on seismic behavior of MSE wall with inclined backfill soils reinforced by polymeric geostrips. *Geotextiles and Geomembranes*, 50(1):116-136. https://doi.org/10.1016/j.geotexmem.2021.09.005

Zheng Y, McCartney JS, Shing PB, et al., 2018. Transverse shaking table test of a half-scale geosynthetic reinforced soil bridge abutment. *Geosynthetics International*, 25(6):582-598. https://doi.org/10.1680/jgein.18.00019